DOE/RL/10236-81/1
(DE82020966)

LIDAR MEASUREMENT OF WIND VELOCITY TURBULENCE SPECTRA ENCOUNTERED BY A ROTATING TURBINE BLADE

By
R. M. Hardesty
J. A. Korrell
F. F. Hall

Work Performed Under Contract No. AC06-80RL10236

NOAA/ERL/Wave Propagation Laboratory
Boulder, Colorado

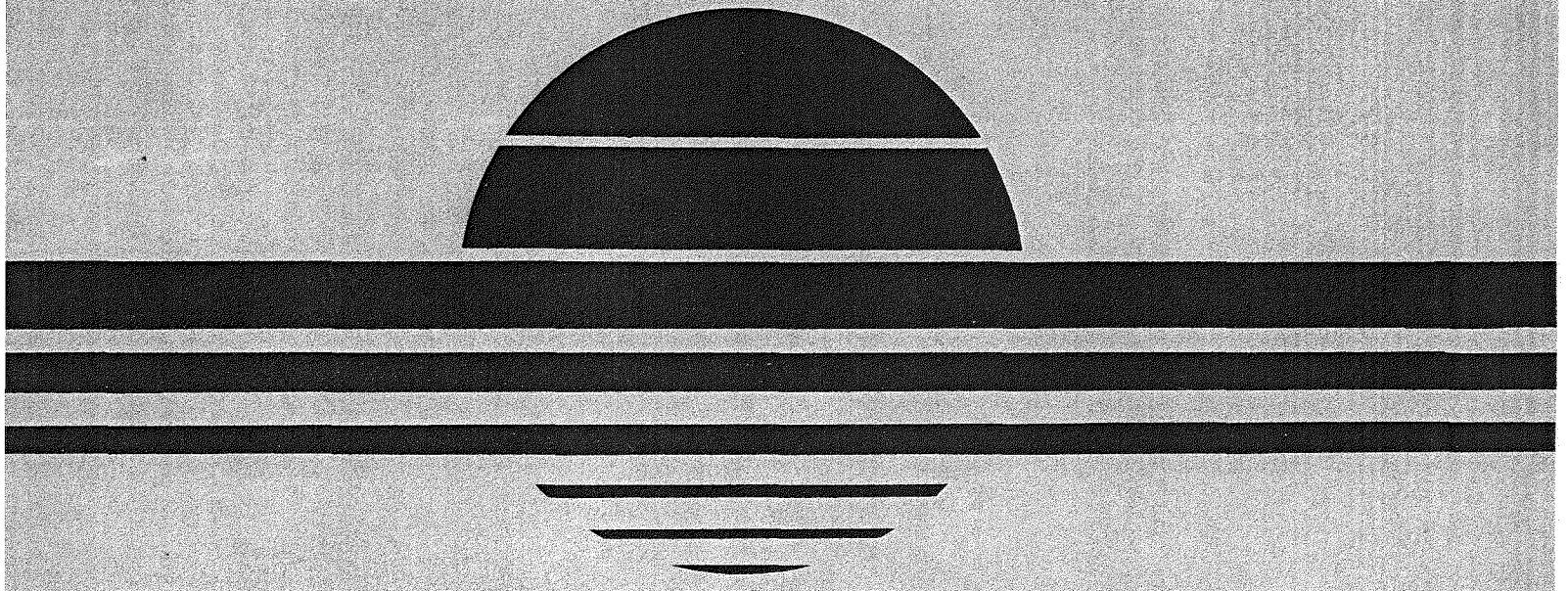

U.S. Department of Energy

Solar Energy

DISCLAIMER

This report has been reproduced directly from the best available copy.

Available from the National Technical Information Service, U. S. Department of Commerce, Springfield, Virginia 22161.

Price: Printed Copy A03
Microfiche A01

Codes are used for pricing all publications. The code is determined by the number of pages in the publication. Information pertaining to the pricing codes can be found in the current issues of the following publications, which are generally available in most libraries: *Energy Research Abstracts, (ERA); Government Reports Announcements* and Index (*GRA* and I); *Scientific and Technical Abstract Reports (STAR);* and publication, NTIS-PR-360 available from (NTIS) at the above address.

DISCLAIMER

DOE/RL/10236-81/1
(DE82020966)
Distribution Category UC-60

LIDAR MEASUREMENT OF WIND VELOCITY TURBULENCE SPECTRA ENCOUNTERED BY A ROTATING TURBINE BLADE

R. M. Hardesty
J. A. Korrell
F. F. Hall

NOAA/ERL/Wave Propagation Laboratory
Boulder, Colorado 80303

Prepared for the United States
Department of Energy
Office of Solar Power Applications
Wind Energy Technology Division

DOE Contract DE-AI06-80 RL10236

CONTENTS

LIDAR MEASUREMENT OF WIND VELOCITY TURBULENCE SPECTRA ENCOUNTERED BY A ROTATING TURBINE BLADE

R.M. Hardesty, J.A. Korrell and F.F. Hall, Jr.
NOAA/ERL/Wave Propagation Laboratory
Boulder, Colorado 80303

ABSTRACT

A homodyne CO_2 lidar system beam was conically scanned around a horizontal axis to measure the wind speed and turbulence characteristics encountered by a rotating turbine blade. Turbulence spectra obtained from the scanning lidar differed considerably from those calculated from fixed-point anemometer measurements, showing a redistribution of energy from lower to higher frequencies. The differences appeared more pronounced during periods when the atmosphere was stable.

I. INTRODUCTION

Considerable attention has been focused recently on the use of large, horizontal axis wind turbines for electric power generation. Mathematical models are often used in the design of such turbines to predict blade loading and control system response under varying wind conditions. Of particular importance is turbine performance during periods of turbulent wind fluctuations. Most models consider fluctuations as discrete wind gusts occurring at some average rate with a particular shape and duration. The fluctuations are assumed to act uniformly over an entire rotor disk. Recently, Thresher et al.[1] and Holley et al.[2] have expanded the scope of turbine models to include turbulent wind fluctuations over length scales smaller than that of the rotor disc diameter. By developing a theoretical turbulence model, then combining it with an advanced horizontal-axis turbine model predicting system response to such a stimulus, they concluded that wind gradients across the rotor disc must be considered as a primary excitation source for such systems.

The turbulence characterization work of Holley et al. is essentially mathematical in nature. There is a need to evaluate sets of experimental data under well measured atmospheric conditions for comparison with the theoretical results. Verholek[3] employed an array of stationary anemometers positioned at intervals around the circumference of an imaginary horizontal-axis rotor disc 24 m in diameter. By sequentially sampling the anemometer outputs at a fixed rate, he effectively measured, with the proper time and space relationship, the winds that would be seen by the tip of a rotating turbine blade. Connell[7] repeated this experiment using a 50 m diameter array. Although this method samples the wind field in the same sequence as a rotating blade, errors may be introduced because of the physical presence of the anemometers and their supports, which produce perturbations in the unobstructed wind flow. Incorporation of a remote sensing measurement technique such as Doppler lidar enables the wind field to be measured to within 0.5 m s^{-1} over the lidar focal volume without the sensor disturbing the normal wind flow. Better circumferential resolution is also obtained, although measurements are volume-averaged rather than single-point measurements.

Doppler lidar methods for remote velocity measurements have been employed in a number of applications.[4,5] In laser anemometry optical radiation transmitted by the laser is scattered from particles which move with the wind flow in the scattering volume. The mean Doppler frequency shift Δf of the scattered radiation is proportional to the mean radial velocity of the aggregate of scatterers in the volume, as

$$\langle \Delta f \rangle = 2\langle V \rangle (\cos \theta)/\lambda \qquad (1)$$

where V is the wind speed, λ the wavelength, and θ the angle subtended by the wind direction and the optical system line of sight. Here the brackets denote ensemble averaging.

In comparisons with stationary anemometers, lidar wind measurements have been shown to give excellent agreement with respect to both correlation of the time series and similarity of the power spectra.[6] During this experiment we used a CO_2 homodyne lidar system and elevated rotating scanner to measure the wind that would have been encountered by the tip of a rotating turbine blade. The objectives of the work were to examine the feasibility and limitations of using scanned Doppler

lidar to gather wind data for input into turbine performance models, and to compare the spectrum of turbulence measured during two-dimensional rotating scans with that measured by a fixed-point anemometer. The experiment was performed under Interagency Agreement DE-A106-80RL10236.

II. EXPERIMENT

To obtain the desired measurement pattern, we irradiated an elevated rotating mirror with the transmitted infrared laser beam, as shown in the schematic of Figure 1. The mirror and its shaft assembly were attached to the movable carriage of the Boulder Atmospheric Observatory (BAO), a 300 m meteorological tower instrumented at eight levels with fast response wind and temperature sensors. By angling the mirror slightly off of the perpendicular relative to the shaft, the lidar beam was made to scan around the base of a horizontal-axis cone whose apex was at the mirror. The transmit beam reflected off the mirror to the scattering volume, where some of its energy was scattered back to the mirror from the atmospheric aerosols and reflected back into the lidar receiver. Since our lidar operated CW for this experiment we varied the range to the scattering volume by changing the focus of the beam. With the carriage fixed at 40 m, and a mirror offset angle of 8.5°, we focused at 70 m to produce a measurement disc 10 m in diameter. This geometry corresponded to a relatively small elevated wind turbine.

The scanner is shown in more detail in the photograph of Figure 2. A torque convertor geared down the motor output to produce a rotation rate of 30 rpm. To simulate turbine performance effectively the wind measurement should be taken with the horizontal scan axis approximately parallel to the mean wind vector. Therefore the entire scanner was mounted on a circular plate which could be rotated to compensate for changes in wind direction. During such adjustments the truck containing the lidar system also was moved and realigned with the scan mirror. In order to avoid measuring winds which had been disturbed by the BAO tower structure, we restricted data collection to periods when the mean wind vector was oriented from the scatterers toward the scanner.

The lidar system, contained in a camper shell fixed to the bed of a pickup truck, employs a homodyne detection scheme for wind velocity measurement. A

portion of the energy from the 10 w, single longitudinal mode CO_2 laser (λ = 10.6 μm) is split off from the main transmit beam and used as the optical local oscillator (LO) signal, which is mixed with the backscattered signal on the cooled HgCdTe detector chip. The detector output current due to the backscattered signal has amplitude proportional to the signal amplitude and frequency equal to the Doppler shift of the backscattered signal. In a homodyne system the sign of the Doppler frequency shift is not recovered; consequently the sign of the radial wind, (i.e., blowing toward or away from the observer) was ambiguous for our measurements. Since most of our data were taken with the system transmit/receive axis oriented directly into the wind, the ambiguity did not pose a problem in data interpretation.

An analog spectrum analyzer with a 100 kHz IF bandwidth was employed to analyze the frequency characteristics of the backscattered signal. Every 100 ms a computer sampled 1024 points of the spectrum analyzer output, plotted the data, and stored it on magnetic tape. Figure 3 shows a typical digitized spectrum of the aerosol backscatter signal. During analysis, we used the computer to calculate the frequency and signal-to-noise ratio (SNR) of the received signal. If the SNR was above a selectable threshold the data point was accepted as valid and included in the analysis. The 100 ms sampling interval provided 20 wind measurements around the imaginary rotor disc.

Although lidar wind measurements have been shown to compare closely with those from anemometers, certain characteristics of the lidar method had to be considered during data analysis and interpretation. The lidar does not measure wind at a point in space, but rather the mean wind over a scattering volume whose diameter and depth increase with the distance to the focus. For this experiment the scattering volume was a narrow cylinder with a diameter of 7 mm and depth of 3.2 m. Thus, some spatial filtering might be expected in the wind data for turbulent eddies with spatial wavelength less than about 3 m. The geometry of the scan configuration also introduced effects that would not exist in fixed-point anemometer measurements. Since the lidar measures radial wind, the effect of the conical scan geometry was to cross couple components of the vertical and transverse wind into the measurement. We can illustrate this undesirable effect by calculating the radial wind measured by the lidar as the beam is scanned conically through

a spatially-varying wind field with linear velocity gradients along the three dimensions. Although the linear gradient model does not sufficiently represent a turbulent wind field, it can be used to show the effect of transverse and vertical components on the wind measurement. Denoting the axial, transverse, and vertical winds as u, v, and w respectively the measured radial wind $r(\theta)$ is

$$\begin{aligned} r(\theta) = \cos\phi\left(u_o + \frac{\partial u}{\partial y} R\cos\theta + \frac{\partial u}{\partial z} R\sin\theta\right) \\ - \sin\phi\left(v_o\cos\theta + \frac{\partial v}{\partial y} R\cos^2\theta + \frac{\partial v}{\partial z} R\sin\cos\theta\right) \\ - \sin\phi\left(w_o\sin\theta + \frac{\partial w}{\partial y} R\cos\theta\sin\theta + \frac{\partial w}{\partial z} R\sin^2\theta\right), \end{aligned} \tag{2}$$

where u_o, v_o, w_o are the wind components at the center of the scanned disc, R is the radius of the disc, x, y and z denote distance in the axial, transverse and vertical directions, ϕ is the cone angle, and θ is the angle with the horizontal made by a radial line from the center of the scan disc to the scattering volume (see Figure 1). Equation 2 shows that non-zero components of transverse and vertical winds and their gradients introduce energy into the first and second harmonics of the measurements proportional to the sine of the cone angle. This illustrates the need to keep the cone angle fairly small to limit the observations to predominantly axial wind effects. During this experiment, the small cone angle of 8.5°, coupled with the fact that the axial wind component was usually at least 5 times the transverse component, allowed us to neglect the effects of crosswind.

The BAO tower not only provided an ideal support for the scanner mechanism, but also supplied data used for comparison with the lidar measurements. Three-axis sonic anemometers and platinum wire thermometers mounted at eight levels from 10 to 300 m and sampled at a rate of 10 Hz give the BAO a unique capability of measuring the turbulent wind and temperature field. Additionally slower-response instruments sampled at 1 Hz defined profiles of temperature, wind speed, and dew point.

As part of the data analysis, we calculated the power spectra for the lidar and tower data using a complex fast Fourier transform (FFT) algorithm. Each lidar run, lasting 20 minutes, resulted in one spectrum consisting of an average of ten 2-minute spectra. The FFT algorithm used the first 1024 points of each 2-minute

period containing 1200 points. Then the complex transform of the time series, X(n), multiplied by its complex conjugate, X*(n), produced the power spectrum, S(n); that is

$$S(n) = X(n)\ X^*(n).$$

Averaging the resulting 512 periodogram points into logarithmically-sized frequency bins smoothed each 2-minute spectrum, ten of which averaged together produced the 20-minute mean spectrum. Finally, as is standard meteorological practice, the power spectral points were multiplied by their frequency and plotted vs. frequency on a log-log scale.

Since the tower operated nearly continuously, we computed one-hour spectra to obtain a more statistically stable estimate of the turbulence field observed by the lidar. Where possible, the one-hour spectrum was centered on the 20 minute lidar spectrum. Spectra longer than 20 minutes are a composite of two spectra. The low frequency end of the spectrum results from a 512 point FFT run on 10 s averaged data, smoothed into frequency bins, and multiplied by frequency. The high frequency end of the spectrum is the averaged 2 min spectra from the 10 Hz data calculated as before. A region of overlap occurs near .025 Hz where agreement is very good.

III. RESULTS

Analysis of the wind measurement data from the lidar and fixed point anemometer indicated that scanning alters the higher frequency (short term) characteristics of the measurement spectrum. Figure 4 shows a 20-s time series record of the lidar-measured wind and the corresponding wind measured by the fixed-point anemometer at a height of 50 m. An obvious sinusoidal component appears in the lidar record principally because of vertical shear of the radial wind across the scanning disk. This component is not present in the fixed-anemometer measured time series. The observed sine wave amplitude is seen to range from approximately .2 to 8 m s^{-1} (peak-to-peak), with a mean amplitude of approximately 0.35 m s^{-1}. The shear corresponding to this value is slightly higher than the .026 s^{-1} mean shear

calculated using measurements from the BAO anemometer at 50 m and 220 m heights. A slight discrepancy between the lidar and anemometer derived shear values should not be unexpected considering the differences in measurement techniques and sensing volumes.

Generally good longer-term sensor comparability is indicated in a 20 minute time series of the 1 s averaged winds measured by the lidar and the 50 m anemometer (Fig. 5). These two data sets show reasonably good long term agreement, an observation that was borne out in the analysis by a coherence calculation, which showed good correlation for frequencies below .01 Hz (100 s period). Lack of coherence at higher frequencies probably resulted because of spatial separation between the two sensors, as well as the difference in measurement technique.

The presence of a harmonic in the scanned lidar wind measurements is obvious in the comparison of spectra calculated from four nearly-sequential time series for the lidar- and anemometer measured winds (Figure 6). While the fixed-anemometer-measured wind spectrum has the familiar $f^{-5/3}$ roll-off over the inertial subrange predicted by Kolmogorov turbulence theory, the harmonic component in the lidar time series produces a large peak in the spectrum at the scanner rotation frequency. We also see traces of higher order harmonics in the lidar spectrum which are probably due to shears in the transverse component, as predicted by Eq. 2. In addition to the harmonic effects, the spectrum of the lidar measurement shows a pronounced reduction in energy relative to the fixed-point anemometer spectrum at frequencies just below the rotational frequency. The two spectra seem to agree at very low frequencies; however at some "cut-off" frequency the lidar spectrum rolls off more sharply relative to that of the anemometer. This deviation increases with higher frequencies up to f_s, the scanning (rotational) frequency. Immediately above f_s, the lidar spectrum appears to have more energy at a given frequency than the corresponding anemometer wind spectrum. This apparent redistribution of energy from lower to higher frequencies was seen in Verholek's results obtained from an anemometer array. More recently it was also pointed out by Connell using data from a 50 m diameter array of anemometers.

We see from figure 6 that the energy decrease at the midrange frequencies in the lidar-measured turbulence spectrum appeared to become increasingly pronounced during succeeding data runs. Examination of BAO-measured wind speed, vertical

wind shear, and stability parameter z/L for each data set (Table 1) showed a gradual increase in stability, along with a slight drop in wind speed, as the measurements progressed. This tends to suggest some correlation; however more data is needed before a conclusion can be reached. In interpreting the results shown in Figure 6, it should be noted that at high frequencies, where turbulence spectra typically are characterized by relatively low energies, the spectral estimates are more susceptible to perturbation by noise in the velocity estimation process. The apparent increase in spectral energy at frequencies greater than 5 Hz in the lidar spectrum may be at least partly a result of more noise in that velocity measurement than in the corresponding anemometer measurement.

IV. DISCUSSION

Our results, showing a decrease in spectral energy at mid-range frequencies for a scanned wind measurement relative to a fixed-point wind measurement, agreed closely with those of Verholek, who performed essentially the same measurement using a circular array of anemometers 24 m in diameter and Connell, whose experiment used a 50 m diameter anemometer array. Connell[7] hypothesized that this apparent redistribution of energy comes about from the rotor blade (or scanning sensor) rapidly chopping across turbulent eddies of a scale size small enough that the velocity varies significantly across the rotor disc diameter. He postulates that shifting of energy generally occurs because the velocity of the rotor tip is usually greater than the mean wind, hence the time required to scan across an eddy or part of an eddy is reduced; and also because the mean eddy dimension $\bar{\lambda}_\theta$ in the direction transverse to the wind may be less than the mean dimension $\bar{\lambda}_u$ along the wind vector. For eddies significantly larger than the disc diameter, the rotor simply spins inside the energy, producing no significant effect.

Spectra calculated from the lidar-measured winds show a substantial reduction in spectral energy at frequencies as low as .001 Hz. If we assume frozen turbulence, then this corresponds to a mean along-the-wind eddy dimension $\bar{\lambda}_u$ of 500 m for our measured mean wind speed of 5 m s^{-1}. Although one might expect the mean transverse eddy dimension λ_θ to be smaller, especially under stable conditions, the fact that some spectral redistribution is occurring for eddy sizes approximately 50 times

larger than the disc diameter indicates that some modification or extension of Connell's hypothesis may be appropriate.

A rather heuristic explanation which appears to fit the data quite well is to assume that sampling a turbulent field at the tip of a rotating blade has the effect of introducing a phase modulation on a sinusoidal waveform. A basic principle of Fourier analysis is that any spectrum may be represented as the sum of many sinusoids at different frequencies, with power proportional to the spectral power at a given frequency of the spectrum. Thus, assuming frozen turbulence we can model the energy at a given frequency f_x in the Eulerian fixed-point spectrum of the axial wind sampled by the anemometer as being produced by a spatially sinusoidal wind field of wavelength λ_{x_o} (λ_u in Connell's notation) being propagated past the sensor by the mean axial wind, where

$$\lambda_{x_o} = \bar{u}/f_x, \tag{3}$$

and $\bar{u}$ is the mean axial wind speed. Since our anemometer measurements sampled the axial wind u(t) in a direction parallel to the mean wind, we can infer no information on the transverse spatial characteristics of u(t) from the measured time series.

In order to examine the effect of scanning the sensor, however our model must include some information on these spatial characteristics. We again apply Fourier analysis principles and invoke Taylor's hypothesis to model the three dimensional wind field as a superposition of three-dimensionally varying sinusoidal fields

$$u(x,y,z) = \sum_{k=1}^{N} \sum_{j=1}^{N} \sum_{i=1}^{N} A_{ijk} \cos\left(\frac{2\pi x}{\lambda_{x_i}} + \frac{2\pi y}{\lambda_{y_j}} + \frac{2\pi z}{\lambda_{z_k}} + \theta_{ijk}\right)$$

where λ_{x_i}, λ_{y_j}, λ_{z_k} are spatial wavelengths along the three system coordinates and A_{ijk} and θ_{ijk} represent amplitude and phase of the three dimensional field defined by the indices i,j, and k.

In our analysis we will analyze the differences between the spectrum obtained by propagating a frozen wind field past a stationary sensor, and that measured by a scanning sensor rotating in the same propagating field. We assume that the fixed sensor is located at the coordinate system axis, while the scanning sensor revolves around it. Then the waveform r(t) measured by a sensor in a frozen field is a function of its position and the mean longitudinal wind speed $\bar{u}$, i.e.,

$$r(t) = u(\bar{u}t + x_s(t),\ y_s(t),\ z_s(t))$$
$$= \sum_{k=1}^{N} \sum_{j=1}^{N} \sum_{i=1}^{N} A_{ijk} \cos\left(\frac{2\pi[\bar{u}t + x_s(t)]}{\lambda_{x_i}} + \frac{2\pi y_s(t)}{\lambda_{y_j}} + \frac{2\pi z_s(t)}{\lambda_{z_k}} + \theta_{ijk}\right), \tag{5}$$

where $x_s(t)$, $y_s(t)$, $z_s(t)$ are the coordinates of the sensor position at time t and we assume $\bar{v} = \bar{w} = 0$. Note that positive $\bar{u}$ is defined in the opposite direction as positive x.

In order to reduce the problem complexity, we analyze the field which produces spectral energy at a specific frequency f_o when propagated past the stationary sensor. This field is characterized by a single spatial frequency variation along the x axis at wavelength λ_{x_o}, where

$$f_o = \frac{2\pi\bar{u}}{\lambda_{x_o}} \ . \tag{6}$$

Fields with other spatial frequencies along the x-axis are neglected, since they do not contribute energy to the stationary-sensor measured spectrum. The time series of the wind measurement from a sensor sampling our single-frequency longitudinal field is

$$r(t) = \sum_{k=1}^{N} \sum_{j=1}^{N} A_{i_o jk} \cos\left(\frac{2\pi(\bar{u}t + x_s(t))}{\lambda_{x_o}} + \frac{2\pi y_s(t)}{\lambda_{y_j}} + \frac{2\pi z_s(t)}{\lambda_{z_k}} + \theta_{i_o jk}\right) \ . \tag{7}$$

Equation (7) essentially includes in the analysis those eddies with characteristic longitudinal size λ_{x_o} and all possible vertical and transverse length scales. This is the complete set of eddies that contribute to the Eulerian spectral point at $f_o = \frac{2\pi\bar{u}}{\lambda_o}$.

We will take our simplification one step further by considering only a single 3-dimensional sinusoidal field with transverse and vertical length scales λ_{y_o} and λ_{z_o}, respectively. The measured time series from such a field is

$$r(t) = A_{i_o j_o k_o} \cos\left(\frac{2\pi(\bar{u}t + x_s(t))}{\lambda_{x_o}} + \frac{2\pi y_s(t)}{\lambda_{y_o}} + \frac{2\pi z_s(t)}{\lambda_{z_o}} + \theta_{i_o j_o k_o}\right) . \tag{8}$$

Our single field approximation enables us to analyze the effect of scanning through a field composed of arbitrary-sized eddies with uniform dimensions. We can set the amplitude and phase terms to unity and zero, respectively, without changing the fundamental principle of the analysis. Under these conditions, the measured time series of wind for a stationary sensor at the origin is, from Equation (8),

$$r(t) = \cos \frac{2\pi\bar{u}t}{\lambda_{x_o}} . \tag{9}$$

If the sensor is moving, the measured time series becomes

$$r(t) = \cos\left(\frac{2\pi\bar{u}t}{\lambda_{x_o}} + \Delta\gamma\right) \tag{10}$$

where

$$\Delta\gamma = 2\pi \left(\frac{x_s(t)}{\lambda_{x_o}} + \frac{y_s(t)}{\lambda_{y_o}} + \frac{z_s(t)}{\lambda_o}\right) \tag{11}$$

is an additional phase modulation resulting from sensor motion across the eddies. For a circular scan, in the y-z plane,

$$\begin{aligned} x_s(t) &= 0 \\ y_s(t) &= R \cos \omega_r t \\ z_s(t) &= R \sin \omega_r t , \end{aligned} \tag{12}$$

where ω_r is the rotational velocity of the scanner and R is the scan disc radius.

Thus

$$\Delta\gamma(t) = \frac{2\pi}{\lambda_{y_o}} R \cos \omega_r t + \frac{2\pi}{\lambda_{z_o}} R \sin \omega_r(t) \tag{13}$$

and the sampled wind becomes

$$r(t) = \cos\left(\frac{2\pi\bar{u}t}{\lambda_{x_o}} + \Delta\gamma(t)\right)$$

$$= \cos\left(\frac{2\pi\bar{u}t}{\lambda_{x_o}} + \frac{2\pi}{\lambda_{y_o}} R \cos \omega_r + \frac{2\pi}{\lambda_{z_o}} R \sin \omega_r(t)\right) \tag{14}$$

which is equivalent to a phase modulated wave

$$r(t) = \cos\left\{\frac{2\pi\bar{u}t}{\lambda_{x_o}} + 2\pi R\left(1/\lambda_{y_o}^2 + 1/\lambda_{z_o}^2\right)^{1/2} \cos(\omega_r t - \pi/4)\right\} . \tag{15}$$

This can be written as the sum of a fundamental plus a number of sidebands as

$$r(t) = \sum_{n=-\infty}^{\infty} J_n(\beta) \cos(\omega_{x_o} t + n\omega_r t) \tag{16}$$

where $J_n(\beta)$ is the Bessel function of the first kind and

$$\beta = 2\pi R\left(1/\lambda_{y_o}^2 + 1/\lambda_{z_o}^2\right)^{1/2}$$

$$\omega_{x_o} = \frac{2\pi\bar{u}}{\lambda_{x_o}} \quad . \tag{17}$$

Examining Eq. 17, we see that as β increases $J_o(\beta)$ decreases and more and more energy is transferred from the fundamental to the sidebands. The spacing of the sidebands equals the rotation frequency, thus energy is transferred to frequencies just slightly higher than the rotational frequency, which seems to agree with our observations. Energy also is transferred to frequencies below the rotational frequency because of the presence of the first sideband of the negative portion of the spectrum (the power spectrum of u(t), or any real signal, is symmetric about zero). Since the value of the function $J_o(\beta)$ decreases appreciably

when $\beta \geq 0.2$, Equation (17) implies that eddies with smaller vertical and transverse scale sizes cause more spectral energy redistribution when monitored with a scanning sensor. The above analysis assumes a field of eddies of a uniform size. In order to predict spectral redistribution in a more realistic atmosphere, we must consider all eddy sizes, i.e.,

$$r(t) = \sum_{k=1}^{N} \sum_{j=1}^{N} \sum_{i=1}^{N} \sum_{n=1}^{\infty} A_{ijk} J_n(\beta_{ijk}) \cos\left\{\frac{2\pi\bar{u}}{\lambda_{x_i}} + n\omega_r t + \theta_{ijk}\right\} \tag{18}$$

where each sinusoid is phase modulated as a function of $\beta_{ijk} = 2\pi R\left(\frac{1}{\lambda_{y_j}^2} + \frac{1}{\lambda_{z_k}^2}\right)^{1/2}$.

The fixed point sampled waveform is, from Equation (7)

$$r(t) = \sum_{i=1}^{N} \sum_{k=1}^{N} \sum_{j=1}^{N} A_{ijk} \cos\left\{\frac{2\pi\bar{u}}{\lambda_{x_i}} + \theta_{ijk}\right\} . \tag{19}$$

Given information about the three-dimensional turbulence characteristics of the atmosphere, we could use Equations (18) and (19) to predict the effect of scanning on the measured power spectrum of r(t). Such a computation is beyond the intended scope of this memorandum. As an illustration however, we can go back to our single-eddy atmospheric model and compare the fixed-point and scanned measurement power spectra at each point. Let our atmosphere consist of eddies with identical scale sizes in each dimension, such that $\lambda_{x_i} = \lambda_{y_i} = \lambda_{z_i}$. Then, for a fixed point measurement

$$r(t) = \sum_{i=1}^{N} A_i \cos\left\{\frac{2\pi\bar{u}}{\lambda_{x_i}} + \theta_i\right\}, \tag{20}$$

while for a scanned measurement

$$r(t) = \sum_{i=1}^{N} A_i \cos\left\{\frac{2\pi\bar{u}}{\lambda_{x_i}} + \frac{2\pi R}{\lambda_{x_i}} \sqrt{2} \cos(\omega_r t - \frac{\pi}{4}) + \theta_i\right\}. \tag{21}$$

If we let $\bar{u}$ = 5 m s^{-1}, R = 5 m, as in the experiment, and assume the turbulence spectrum is Kolmogorov, such that

$$A_i^2 \propto f^{-5/3} ,$$

we can calculate the scanned and fixed-point measured spectra. Figure 7 shows the results of these calculations using the zeroth and first order Bessel functions in Equation (16). Even though we considered only a small fraction of the total turbulence field, the calculated spectrum bears a remarkable resemblence to the experimental measured spectrum of Fig. 6. This is not so surprising when one considers that while most of the effect of scanning comes from the smaller eddies, most of the energy is in the large eddies. Since for a Kolmogorov spectrum, the spectral amplitude A_{ijk} typically rolls off faster than $J_n(\beta_{ijk})$, the effects of the large eddies will dominate. Inclusion of other eddy sizes in the model will probably moderate some of the extreme excursions seen in Fig. 7.

The preceding hypothesis is strongly based on the concept that phase coherence of the measured wind speed exists, at least in the mean sense, simultaneously over all three dimensions of a turbulent eddy. There appears to be a scarcity of data in the literature to either support or refute this assumption. In our analysis of data from the BAO fixed anemometers, we found that the cospectra calculated from the 22 and 50 m anemometer measurements showed a strong correlation out to frequencies of .01 Hz, implying some vertical coherence of horizontal wind measurements. The data taken from previous circular anemometer arrays, if still available, could be analyzed to gather more information on this matter.

The objectives of this experiment, those of demonstrating the concept and accumulating a data set for a given geometric configuration, represented essentially a first cut at the problem. Redoing the measurements at a variety of scan rates and cone angles should provide more insight on the parameterization of the observed effects. Certainly, additional anemometers displaced in the transverse direction during the lidar measurements would address the validity of the phase modulation model.

Throughout the course of these measurements we were periodically hampered by long periods when the wind direction was such that the tower perturbed the mean

wind field enough to preclude gathering of good data. Additionally, frequent periods of downslope westerly winds tended to be characterized by such low turbidity that our sensitivity-limited system at times could not accurately measure the backscattered signal. Consequently the data available for analysis, although consistent, were limited. Since these measurements, the coherent lidar program area has assembled a lidar system with 20-30 dB greater sensitivity which has the capability to gather large amounts of data during virtually any type of conditions. Such a system would be ideal for a more ambitious second stage of this experiment.

V. ACKNOWLEDGMENTS

We wish to acknowledge the excellent assistance of Chris Wylie in the scanner design and data collection effort, and to thank Chandran Kaimal for his valuable suggestions and comments regarding the observed spectral energy redistribution in the scanned lidar wind measurements. Jim Connell provided the original stimulus for conceiving and performing this investigation.

Table 1.--Atmospheric Parameters Measured during Data Runs Analyzed for Figure 6.

Run	Time	Mean Longitudinal Wind ($m\ s^{-1}$)	z/L	22 m-50 m shear (m^{-1})
a	1404-1424	5.4	-0.5	.012
b	1446-1506	4.7	-0.5	.008
c	1540-1600	4.7	$\sim$0	.019
d	1610-1630	4.5	1.0	.026

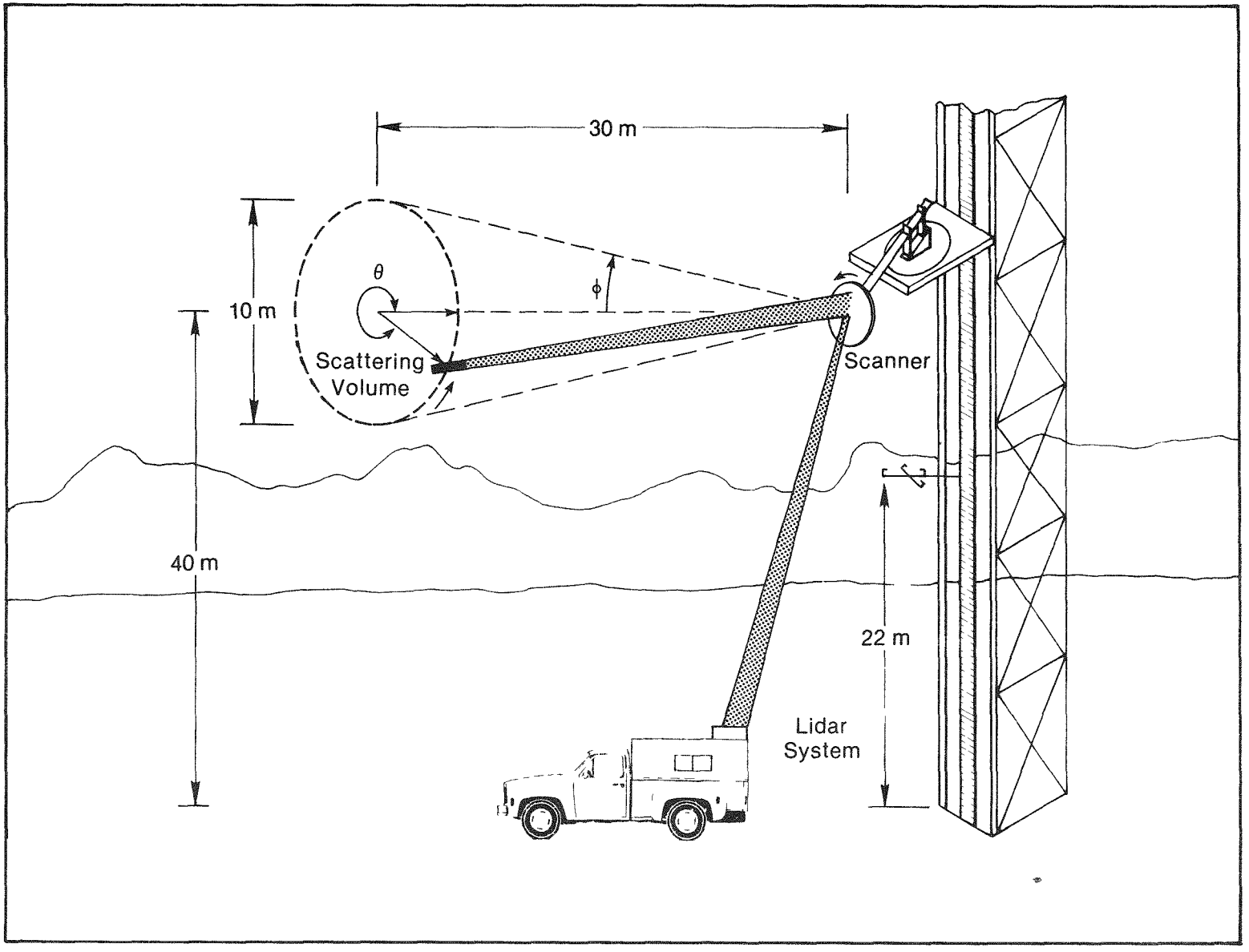

FIGURE 1. Schematic of Measurement Configuration Showing Pickup Camper-Mounted Lidar System, Scanner, and BAO Tower

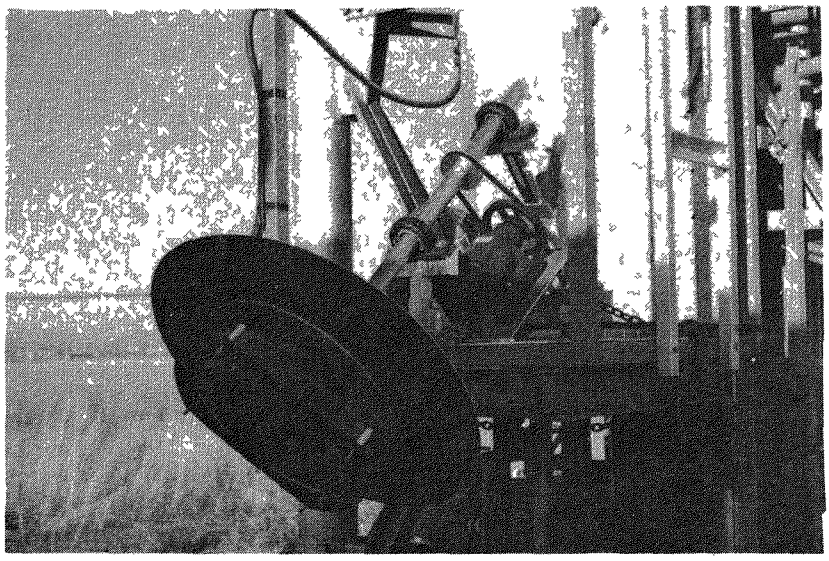

FIGURE 2. Photograph of Nutating Mirror and Associated Scanner Hardware Mounted on BAO Carriage

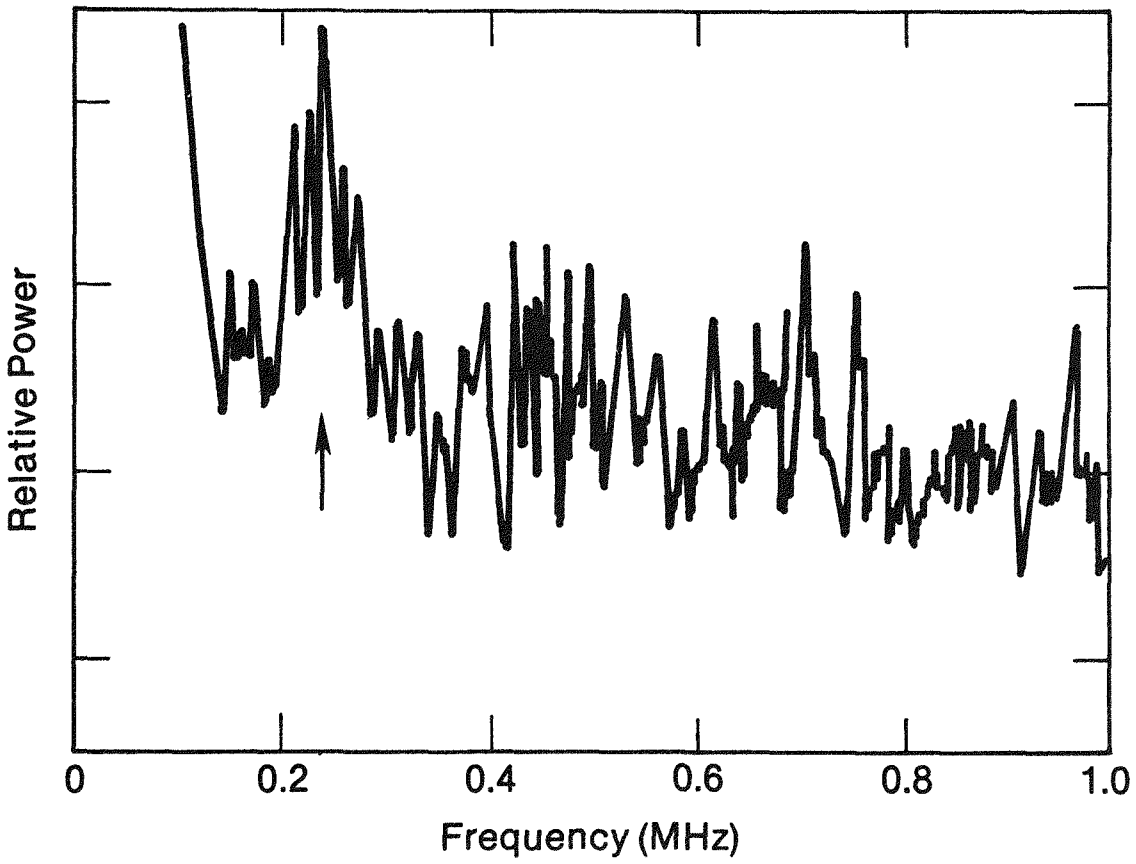

FIGURE 3. Digitized Analog Spectrum Analyzer Sweep Showing the Lidar-Measured Wind Signal (Arrow) at 0.225 MHz. Large spectral values of frequencies below 0.1 MHz result from spectrum analyzer DC artifact.

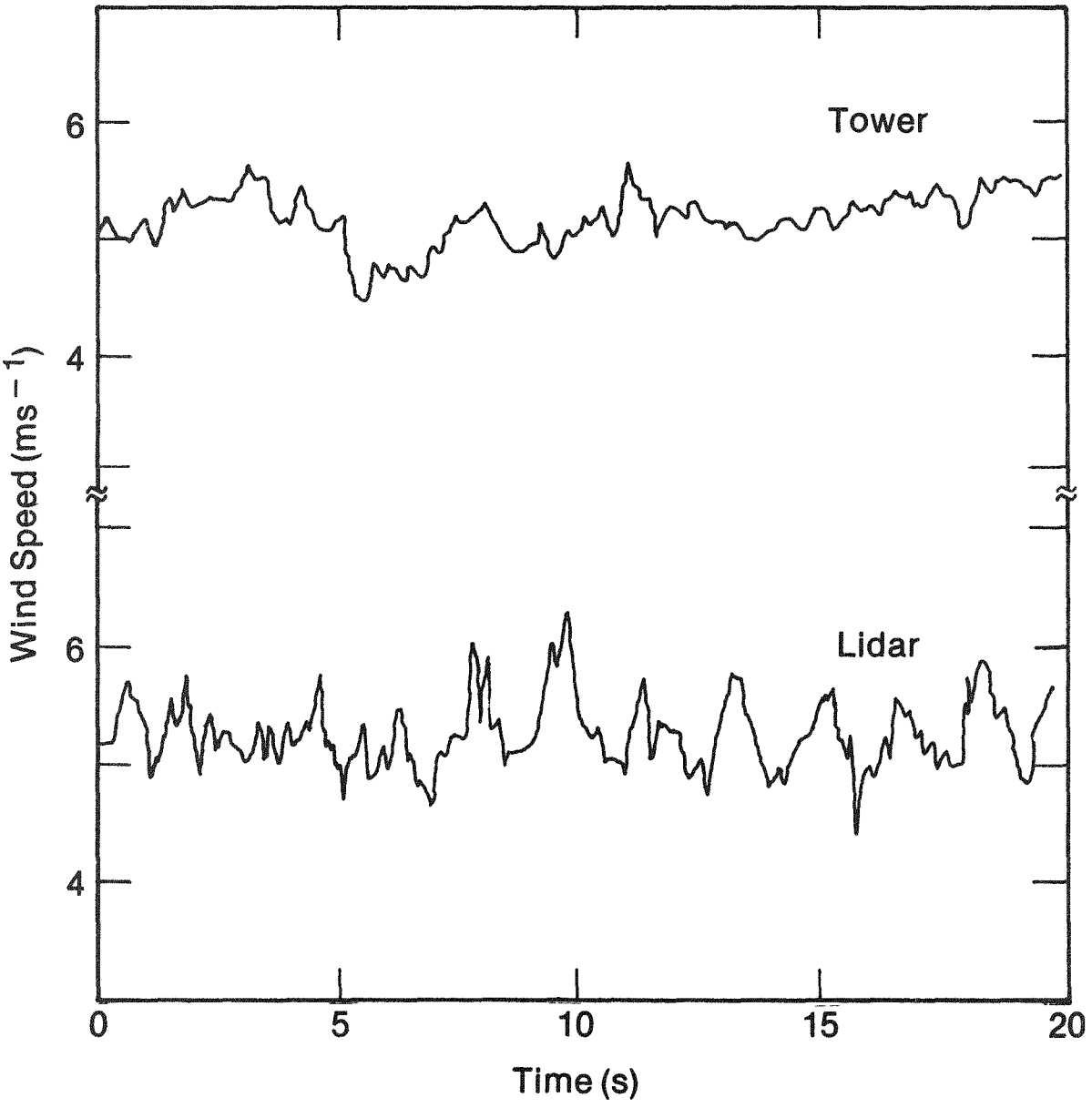

FIGURE 4. 20 s Time Series of Lidar and 30 m Height Tower Anemometer-Measured Winds Showing Sinusoidal Component in Lidar Measurement. The two traces are not necessarily exactly time aligned.

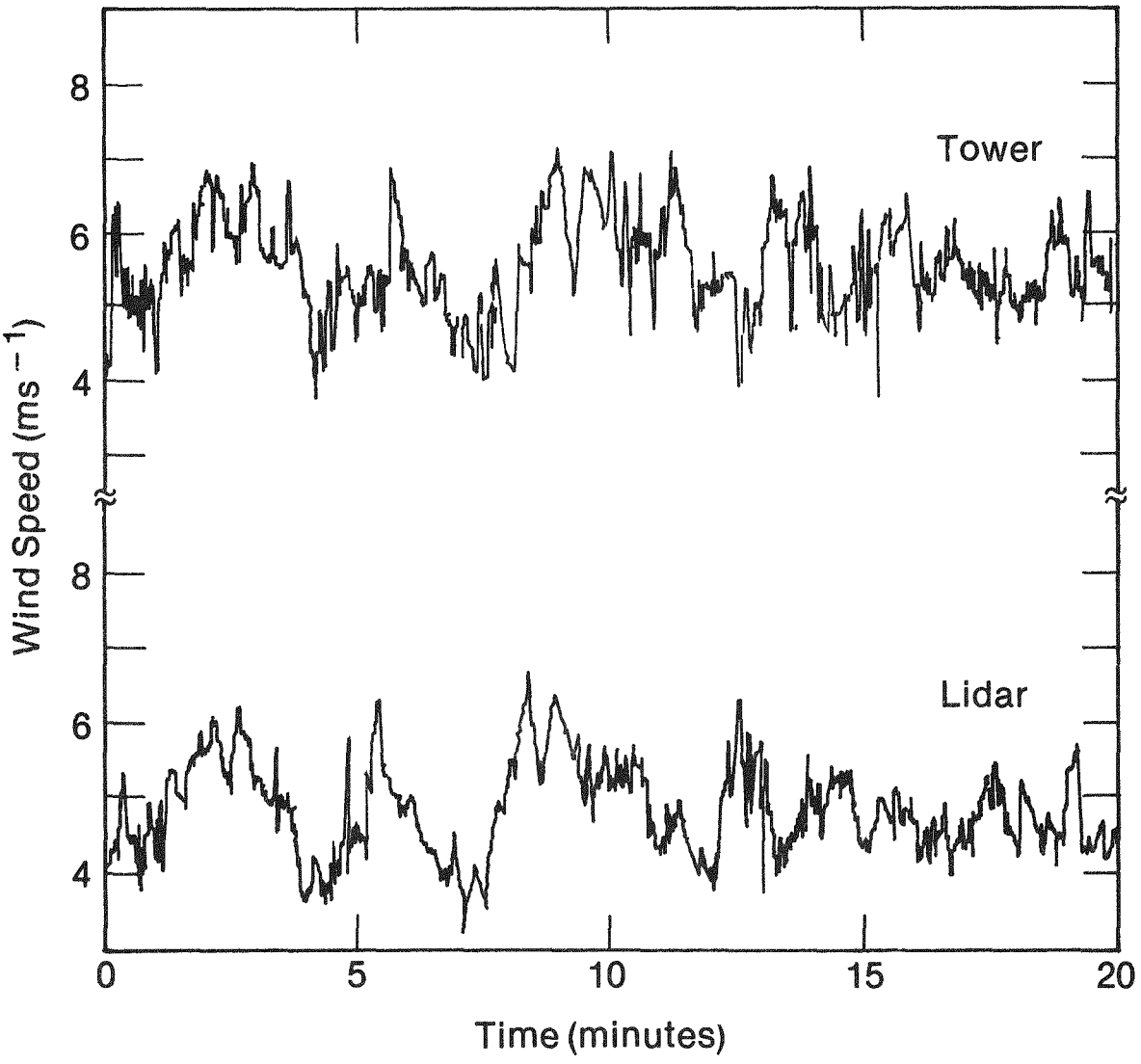

FIGURE 5. 20 Min Record of Lidar and 1 s Average, 50 m Height Tower Anemometer Wind Measurements Showing Close Similarity of Long Term Measurement

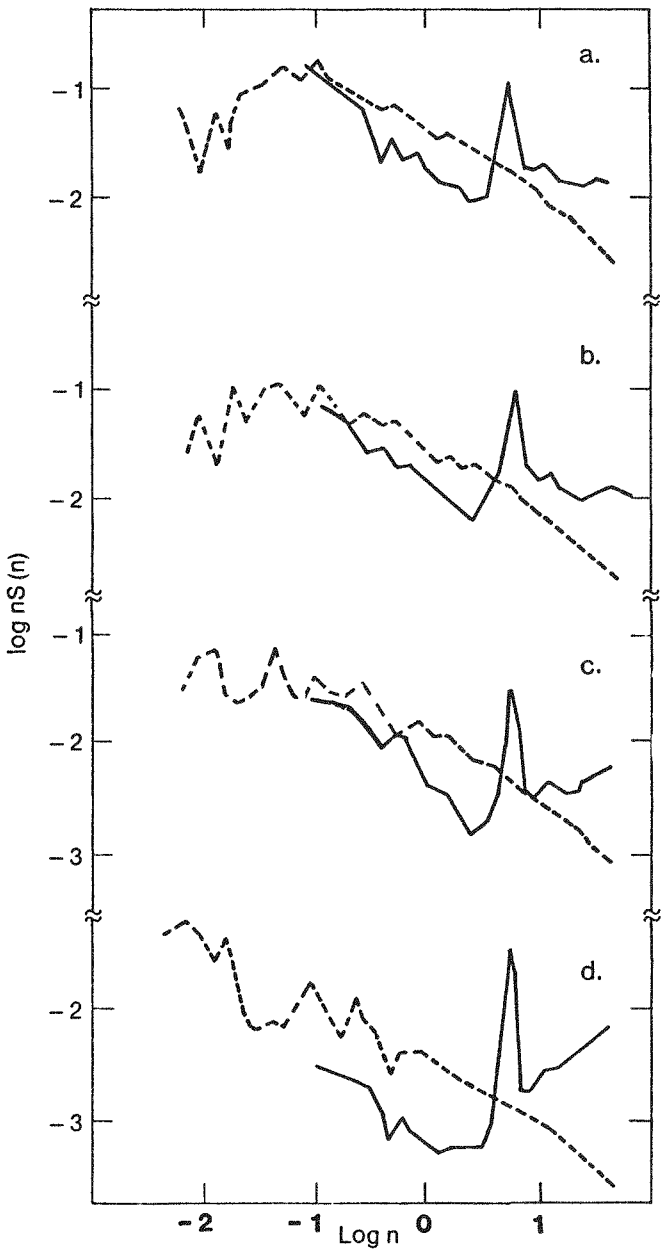

FIGURE 6. Sequence of Wind Velocity Spectra Calculated From Anemometer Measurements (Broken Line) and Lidar Measurements (Solid Line). The alphabetic labels refer to the description of parameters in Table 1.

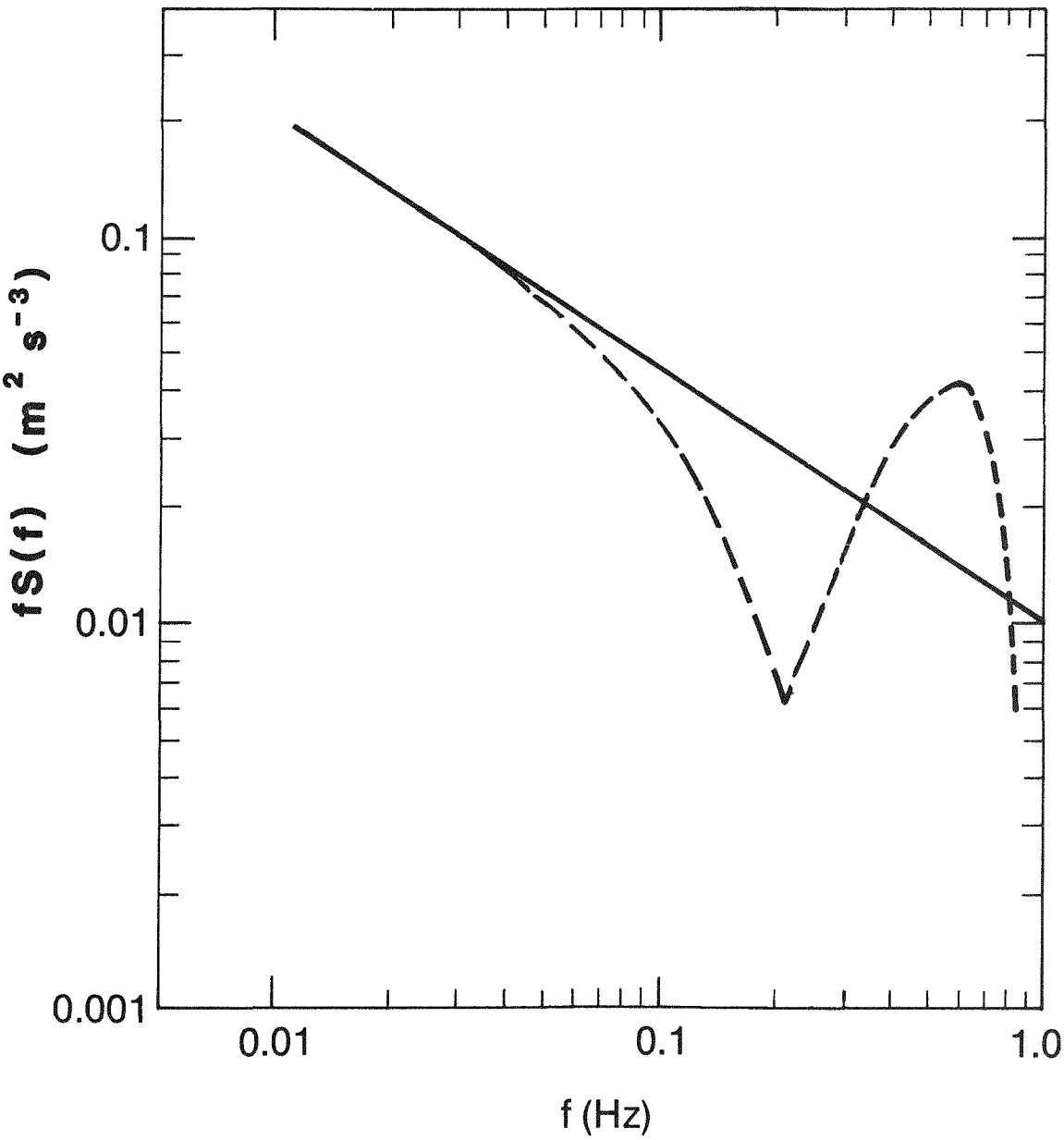

FIGURE 7. Theoretical Spectrum of Turbulence for Typical Fixed-Point (Solid Line) and Rotationally Scanned (Dashed Line) Wind Measurements. The fixed-point spectrum has $f^{5/3}$ slope characteristic of Kolmogorov turbulence. The rotationally scanned spectrum was calculated assuming phase correlation across turbulent eddies.

REFERENCES

1. R.W. Thresher, W.E. Holley and N. Jaferey, Proc. Second DOE/NASA Wind Turbine Dynamics Workshop, Cleveland, Ohio (1981).

2. W.E. Holley, R.W. Thresher and S.-R. Lin, Proc. Second DOE/NASA Wind Turbine Dynamics Workshop, Cleveland, Ohio (1981).

3. M.G. Verholek, "Preliminary Results of a Field Experiment to Characterize Wind Flow through a Vertical Plane," Battelle Tech. Report PNL-2518, (1978).

4. R.L. Schwiesow and R.E. Cupp, Appl. Opt., 15, 1 (1976).

5. R.L. Schwiesow, J. Appl. Meterol. 20 (1981).

6. T.R. Lawrence, D.J. Wilson, C.E. Cravan, I.P. Jones, R.M. Huffaker, J.A.L. Thomson, Rev. Sci. Instr., 43, 512 (1972).

7. J.R. Connell, "Turbulence Spectrum Observed by a Fast-Rotating Wind Turbine Blade," Battelle Tech. Report PNL-3426 (1980).

☆U S GOVERNMENT PRINTING OFFICE 1982 646 069/188